Protofibril Assemblies of the Arctic, Dutch, and Flemish Mutants of the Alzheimer's Aβ_{1-40} Peptide

Nicolas Lux Fawzi,* Kevin L. Kohlstedt,‡ Yuka Okabe,† and Teresa Head-Gordon*†§

*UCSF/UCB Joint Graduate Group in Bioengineering, Berkeley, California 94720; †Department of Bioengineering, University of California, Berkeley, California 94720; ‡Department of Chemical and Biological Engineering, Northwestern University, Evanston, Illinois 60208; and §Physical Biosciences Division, Lawrence Berkeley National Laboratory, Berkeley California 94720

ABSTRACT Using a coarse-grained model of the Aβ peptide, we analyze the Arctic (E22G), Dutch (E22Q), and Flemish (A21G) familial Alzheimer's disease (FAD) mutants for any changes in the stability of amyloid assemblies with respect to the wild-type (WT) sequence. Based on a structural reference state of two protofilaments aligned to create the "agitated" protofibril as determined by solid-state NMR, we determine free energy trends for Aβ assemblies for the WT and FAD familial sequences. We find that the structural characteristics and oligomer size of the critical nucleus vary dramatically among the hereditary mutants. The Arctic mutant's disorder in the turn region introduces new stabilizing interactions that better align the two protofilaments, yielding a well-defined protofibril axis at relatively small oligomer sizes with respect to WT. By contrast, the critical nucleus for the Flemish mutant is beyond the 20 chains characterized in this study, thereby showing a strong shift in the equilibrium toward monomers with respect to larger protofibril assemblies. The Dutch mutant forms more ordered protofilaments than WT, but exhibits greater disorder in protofibril structure that includes an alternative polymorph of the WT fibril. An important conclusion of this work is that the Dutch mutant does not support the agitated protofibril assembly. We discuss the implications of the structural ensembles and free energy profiles for the FAD mutants in regards to interpretation of the kinetics of fibril assembly using chromatography and dye-binding experiments.

INTRODUCTION

Alzheimer's disease (AD) is characterized by the appearance of neuritic plaque deposits comprised primarily of amyloid β peptide (1), whose chemicophysical properties are central to understanding the disease state. Amyloid β is created by proteolytic cleavage of the amyloid precursor protein (APP), as a 40 or more virulent 42 residue sequence (Aβ_{1-40} or Aβ_{1-42}) with unknown function (1,2). Although many familial Alzheimer's disease (FAD) mutants of the APP protein are external to the Aβ peptide sequence and typically influence Aβ processing, a set of mutants that cluster near amino acid positions 21 through 23 in the amyloid β peptide itself have drawn special attention due to possible changes of peptide biochemistry (1). Some of the most well-studied FAD mutants of amyloid β include the Dutch (E22Q) (3,4), Flemish (A21G) (5,6), Italian (E22K) (7,8), Arctic (E22G) (9), Iowa (D23N) (10), and double Dutch/Iowa mutants (E22Q, D23N) (10), all of which have been characterized for both Aβ_{1-40} and Aβ_{1-42} both in vitro and in vivo. Despite the locality of the mutation, the FAD mutants show dramatic diversity in presence or absence of AD dementia symptoms and intracerebral hemorrhaging (10), exhibit variations in Aβ_{1-42} levels in media from cells transfected with a given mutant (9), and show strong differences in the regions of the brain tissue or vasculature in which amyloid plaques are deposited (9,11).

More relevant to this study are the strong differences in the kinetics of the formation of fibril assemblies of WT and mutant Aβ that make up the amyloid plaque (12–15). In vitro studies have found that the Dutch mutant nucleates and fibrillizes more readily than WT, that the Arctic mutation has a higher propensity to form protofibrils (either distinct from, or precursors to, the fibril state) although fibrillization rates are comparable to WT, whereas the rate of fibril formation is greatly reduced for the Flemish mutant relative to WT (9). Morelli et al. showed that proteolytic enzymes more easily degrade monomeric WT Aβ, Italian, and Flemish mutants, whereas proteolysis of the Arctic and Dutch mutant protein is not as efficient-likely due to their rapid sequestration into protofibril or fibril morphologies that inhibit degradation by the enzyme (16). Although in vitro experiments have shown that different polymorphs of the mature Aβ fibril can contribute to variation in cell viability (17), and synaptic activity is greatly impaired in the presence of the insoluble plaque (18), biochemical evidence is accumulating that immature and/or soluble oligomer states may be the more prevalent cytotoxic species (19–23). Again, the FAD mutants show distinct differences; cognitive deficits arising from the Arctic mutant were traced to a nonfibrillar form of the Aβ peptide, whereas the severity of memory loss symptoms for carriers of the Dutch mutation were consistent with interference from the mature fibrillar Aβ species (24).

A convenient separation of the soluble oligomers and mature fibril regimes may be gleaned from the mechanism of fibrillization of full length WT Aβ peptides that has been shown to follow a nucleation-dependent polymerization

Submitted September 7, 2007, and accepted for publication October 30, 2007.

Address reprint requests to Teresa Head-Gordon, E-mail: tlhead-gordon@lbl.gov.

Editor: Ruth Nussinov.

0006-3495/08/03/2007/10 $2.00

doi: 10.1529/biophysj.107.121467

mechanism (13,25–27). The kinetic model developed by Ferrone (28) assumes that the observed lag phase is due to the formation of a critical nucleus—the assembly of monomers into a certain oligomer size corresponding to the largest free energy barrier—beyond which a gradient of favorable free energy or ''downhill'' polymerization progresses into a mature fibril. However, the structural characteristics and oligomer size of the soluble nucleating species have yet to be determined experimentally for either the WT or familial mutants, and the mechanism of polymerization that eventually delineates a mature fibril is unclear.

A number of important computational studies have addressed the monomer conformation and oligomers assemblies of the WT and FAD mutants, both on the full length sequence as well as Aβ fragments (29–43). We have chosen in this study to focus on the Aβ_{1-40} peptide because the best quality experimental structural data is available for this system (17,44–46). Given the ability of Aβ_{1-42} and Aβ_{1-40} to cross seed fibril growth, we believe the Aβ_{1-40} structure is relevant to the fibril form of Aβ_{1-42}.

We have recently developed (47) and used a coarse-grained protein model to characterize the critical nucleus, structural stability, and fibril elongation propensity of WT Aβ_{1-40} protofibrils (48). We pursue a coarse-grained C_α model unlike previous all-atom studies because these models enable us to retain physico–chemical interactions through model physics faithful to the true system while enabling a full statistical characterization of the ensemble properties for each mutant, something not attainable for much more computationally expensive all atom models. These coarse-grained models capture both sequence specific interactions and geometrically accurate α-helical and β-sheet secondary structure geometries while retaining the simplicity of a C_α protein model (see Methods). By careful parameterization of the interaction potentials between coarse grained amino acid positions, these models capture well the excluded volume and hydrophobic interactions of the true system. The inclusion of a direction dependent backbone hydrogen bond potential enables the model to capture cooperative assembly of secondary structures with faithful β-sheet geometry resulting in native state RMSD of ~3 Å for globular proteins relative to experimental NMR structures (47). Although favorable opposite charge interactions can be modeled as attractive interactions, this model is limited by the lack of explicit electrostatic interactions and we leave the analysis of specific charged interactions to future studies with an enhanced model. We have previously characterized this model for the WT sequence and carry out all analysis of mutants as comparisons to this sequence. Within our model we have represented two different quaternary symmetry forms proposed by solid state NMR for so-called ''agitated'' fibrils (17,44–46). As shown in Fig. 1, the cross section of the fibril is made up of two ''U-shaped'' monomers with hydrophobic C-terminal regions in van der Waals contact in a pseudo-symmetry C_{2z} form, and larger (proto)fibril peptide assemblies propagate this dimer motif down the fibril axis. Our nomenclature is to define a (proto)fibril as being composed of two (proto)filaments of in-register parallel intermolecular N-terminal and C-terminal β-sheet regions that can be organized by the C_2 symmetry operation about the fibril z axis (Fig. 1). Protofibril refers to a fibril that is well below micron-size lengths.

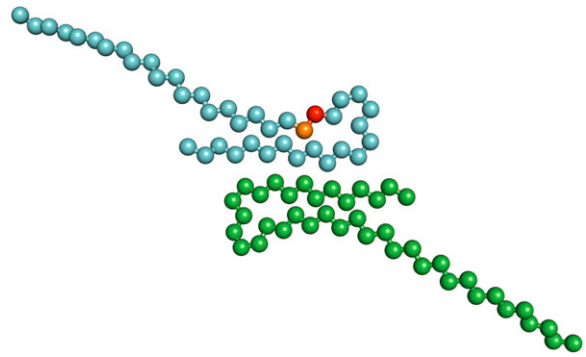

FIGURE 1 Ideal cross section of agitated fibril morphology. The two monomer cross section of the bead model with C_{2z} symmetry based on SS-NMR data (17, 31–33) after equilibration within a large WT fibril (40-chain). Ala 21, site of the Flemish mutation, is pictured in orange on one monomer. Glu-22, site of Arctic and Dutch mutations, is pictured in red.

Given this model, we calculated equilibrium populations of structurally stable and unstable protofibrils for WT Aβ_{1-40} as a function of the number of dimer cross sections, and evaluated a free energy profile for monomer-protofibril equilibrium (48). We determined a critical nucleus of 10 chains for WT Aβ_{1-40}, characterized as having well formed intermolecular β-sheets, but lacking structural integrity at the C-terminal interface so that the protofilaments do not align along the fibril axis (48). Beyond the critical nucleus, we found that 16 monomer chains showed the fibril extension propensities of a mature fibril, for the reason that a sufficient hydrophobic density is reached to stabilize the C-terminal interface and therefore align the protofilaments along the fibril axis. At this length, the $\Delta\Delta G$ for cross-section addition is a constant and defines polymerization equilibrium as shifted strongly in favor of the fibril form. Thus the oligomer size below or above 10 chains for WT Aβ delineate the concentration conditions for further study as to whether the cytotoxic species correspond to early soluble aggregates or mature insoluble (proto)fibrils (48).

In this work, we extend our coarse-grained model study of amyloid assemblies of WT Aβ to the Dutch, Flemish, and Arctic FAD mutants. Our work starts with the assumption that the best experimental model of the complete WT Aβ_{1-40} amyloid fibril, derived from fibrils prepared under ''agitated'' conditions (17,44–46), is also an appropriate structural model of these FAD mutants. An important component of this work is to test whether the agitated fibril morphology is an appropriate model for mutations at positions 21 and 22. Given the importance of the salt bridge defined by D23 and K28 in stabilizing the agitated fibril assemblies, the Italian and Iowa FAD mutations at position 23 that lose the ability to

neutralize charge will be unlikely to conform to the reported SS-NMR agitated structure (46), and are not considered in this study but have been examined recently by Zheng et al. (43).

We find that the free energy trends for Aβ assemblies among the familial and WT sequences show that the structural characteristics and size of the critical nucleus shifts dramatically among the mutants, even though the single point mutations are localized in the same region of the Aβ peptide. The Arctic mutant's disorder in the turn region introduces new stabilizing interactions that better align the two protofilaments to yield a well-defined fibril axis. By contrast, we find that the critical nucleus for the Flemish mutant is beyond the 20 chains characterized in this study, thereby indicating a strong shift in the equilibrium toward monomers with respect to larger ordered protofibril assemblies. We find that the Dutch mutant forms more ordered protofilaments than WT, but more disorder in protofibril structure that includes an alternative polymorph of the WT fibril. We discuss the implications of the structural ensembles and free energy profiles for the FAD mutants in regards to interpretation of the kinetics of fibril assembly using chromatography and dye-binding experiments (9,49).

METHODS

Coarse-grained protein model

The coarse-grained model we developed has been used to study the folding and aggregation properties of members of the ubiquitin α/β fold class (50–55), and we have updated it recently to improve its faithfulness to real proteins while retaining its simplicity (47). The coarse-grained model consists of an unbranched chain of beads, each representing a single amino acid. Beads are assigned interaction type and strength using a Lennard-Jones functional form based on a mapping from the 20 amino acids to our four bead types: B, strong attraction; V, weak attraction; N, weak repulsion; and L, strong repulsion. Interactions between beads three or more positions apart are represented by potentials of mean force corresponding to bead flavor, and solvation water is treated implicitly by incorporating favorable interactions between hydrophobic groups. Bonds between beads are kept rigid at one reduced distance unit (~3.8 Å) representing the distance between C_α positions in a peptide chain. Angles formed by three consecutive beads are represented by a harmonic potential with mean 105°, the average of the C_α pseudo bond-angle in extended and helical secondary structures. A single torsional potential, ''S'', which has competing minima for helical (~60°) and β-sheet (~180°) arrangements is applied for every dihedral angles formed by four consecutive beads with the exception of some of the dihedral angles where one of the central beads is a glycine in the 20 amino acid sequence. For these dihedrals, we replace the helical/extended torsional potential with a ''floppy'' potential, ''T'', where the barriers to transition between helical and extended type angles are reduced, in this way capturing the greater conformational flexibility of the peptide chain near glycine residues. We have used this model to differentiate sequence driven folding mechanisms of proteins L and G with ~3 Å RMSD models to the native PDB structures (47), as well as determine the critical nucleus and fibril elongation propensity of the wild-type Aβ_{1-40} fibrils. We refer the reader to our recent work (47,48) for full specification of the model applicable to this study.

A model of an amyloid dimer cross section was constructed in the single-bead representation of our model according to the constraints specified by Petkova et al. (45). Because this model is a single-bead representation of a protein, the (ϕ,ψ) angle constraints were converted into local secondary structure assignments and then applied to the model. The resulting 20-letter sequence of the WT Aβ_{1-40} peptide and the corresponding coarse-grained (CG) primary and secondary structure are:

```
1°sequence      DAEFRHDSGYEVHHQKLVFFAEDVGSNKGAIIGLMVGGVV
1°sequence (CG) LVLBLNLNNBLVNNLNBVBBVLLVNNLNNVBBNBBVNNVV
2°structure (CG)  SSSSSSSSSSSSSSSSSSSTTSSTTSSSSSSSTT.
```

We highlight in bold what aspects of the model change under the Arctic (E22G) or Flemish (A21G) mutations. The amino acid sequence and secondary structure assignment for our model of the Flemish Aβ peptide (A21G) is

```
1°sequence      DAEFRHDSGYEVHHQKLVFFGEDVGSNKGAIIGLMVGGVV
1°sequence (CG) LVLBLNLNNBLVNNLNBVBBNLLVNNLNNVBBNBBVNNVV
2°structure (CG)  SSSSSSSSSSSSSSSSSSTTSSTTSSTTSSSSSSTT
```

that changes a bead with small attraction to one of small repulsion, while making the dihedral angles in that vicinity of the chain floppier given the greater conformational flexibility of the glycine backbone. Correspondingly, the amino acid sequence and secondary structure assignment of the Arctic Aβ peptide (E22G) is:

```
1°sequence      DAEFRHDSGYEVHHQKLVFFAGDVGSNKGAIIGLMVGGVV
1°sequence (CG) LVLBLNLNNBLVNNLNBVBBVNLVNNLNNVBBNBBVNNVV
2°structure (CG)  SSSSSSSSSSSSSSSSSSTTSTTSSTTSSSSSSTT.
```

This also makes the dihedral angles floppier, but in a region of the chain shifted by one amino acid, while at the same time changing a more strongly repulsive bead interaction to a weaker one. Finally, because the Dutch Aβ peptide mutation (E22Q) does not involve a mutation to glycine, the glutamine mutation is represented only at the level of a primary sequence

```
1°sequence      DAEFRHDSGYEVHHQKLVFFAQDVGSNKGAIIGLMVGGVV
1°sequence (CG) LVLBLNLNNBLVNNLNBVBBVLVNNLNNVBBNBBVNNVV
2°structure (CG)  SSSSSSSSSSSSSSSSSSSSTTSSTTSSSSSSSTT
```

in which an L bead that describes repulsion due to the alignment of negative charge down each of the protofilaments is changed to a V bead that qualitatively makes the interactions attractive. We justify this change from L bead to attractive V to represent E22Q by noting that glutamine-glutamine interactions of this geometry are favorable in polyglutamine aggregates (56). Globular proteins that contain a sequence run of glutamines are known to form β-sheets that are stabilized by hydrogen bonds between carbonyl and amide moieties of the glutamine side chain chemistry as well as hydrophobic interactions between aligned nonpolar regions of the glutamine side chains, and polyglutamine fibrils show similar hydrogen bonding patterns that stabilize the intermolecular assemblies (56).

These three mutations, Flemish, Arctic, and Dutch have clear coarse-grained bead and dihedral mutations that we have described above. Representing change of charge mutations from acidic to basic amino acids such as the Italian mutation (E22K) are difficult to represent in our current formulation of the coarse-grained model that does not include explicit treatment of electrostatic effects. We believe that the mutations we have pursued here capture the type of change that would be seen in the full atomistic system because the perturbation of the WT system, to which we always compare in its coarse-grained form, is well represented by the mutations. We note that the Artic and Dutch mutations do result in a change in the charge of the peptide that undoubtedly influences monomer and disordered oligomer thermodynamics and dimerization kinetics in a pH and salt dependent manner. Our study, however, aims to examine how these mutations, local changes to the sequence represented well by bead and backbone dihedral angle differences, affect the global structure and thermodynamics of the protofibril and fibril assemblies in standard physiological buffer conditions for which our original model has been parameterized.

Model building

To construct the amyloid fibril, in-register parallel intermolecular β-sheet models were made with 40 starting chains for the C_{2z} form. Each strand in the

models contains a disordered N-terminal region (residues 1–9), an N-terminal β-sheet region (residues 10–24), a turn region (residues 25–29), and a C-terminal β-sheet region (residues 30–40). In comparison to the original model of a fibril presented by Tycko et al. (45), we have the C-terminal β-strand ''flipped'' in orientation, where the residues packed against the N-terminal β-strand are even numbered, as determined by the most recent NMR data (46). Models were built with N- and C-terminal strands without stagger, but interdigitation of structures into staggered structures can be seen in equilibrated structures at finite temperature. Once equilibrated, the beads representing the N- and C-terminal β-sheets interdigitate to form contacts internal to each subunit of the fibril with a particular value of ''stagger''(46). The most recent solid state NMR work has suggested that the stagger is either STAG(+2) or STAG(−2) (46), although our models under thermal equilibration give STAG(−1) (48). Models for different seed sizes (4,6,8,10,12,14, 16,18,20) were created by retaining the inner-most chains from the equilibrated 40-chain starting structures to ensure that edge effects (loss of perfect fibrillar order of the exterior chains) were not incorporated into the seeds.

Simulation protocol

We use constant-temperature Langevin dynamics with friction parameter $\zeta = 0.05$. Bond lengths are held rigid by using the RATTLE algorithm (57). All simulations are carried out in reduced units, with mass m, energy ε_H, and k_B all set equal to unity. The 40-chain C_{2z} fibril models were equilibrated with Langevin dynamics at a temperature of 0.45 for 1500τ (300,000 steps). This procedure was repeated between 50 (Arctic and Flemish) and 100 (WT and Dutch) times so that the stochastic dynamics generated 50 or 100 equilibrated starting structures of a 40-chain fibril seed for C_{2z}; 1–3 simulations of each of the 50–100 models were run for 5000τ (1,000,000 steps) at $T^* = 0.45$ ($T \approx$ 337K).

The reported protofibril stability data are based on statistics collected ~50–150 independent simulations per chain number. Statistics on the chain conformation were gathered every 50τ (10,000 steps). Structural stability for each time point was quantified by two different variants of the χ parameter:

$$\chi = \frac{1}{M}\sum_{\alpha=1}^{N_c}\sum_{\beta>c}^{N_c}\sum_{i}^{N}\sum_{j}^{N} h\left(\varepsilon - |r_{\alpha,i;\beta,j} - r^0_{\alpha,i;\beta,j}|\right). \quad (1)$$

The generic χ parameter evaluates the sum over bead i on chain α and bead j on chain β and α and β range over the N_c chains making up the exterior and neighboring chains on each end, h is the Heaviside step function, ε is the tolerance set to 0.5 distance units (~1.9Å), $r_{\alpha:i;\beta:j}$ is the distance between bead i on chain α and bead j on chain β, $r^0_{\alpha:i;\beta:j}$ is the pair distance in the initial structure, and M is a normalizing constant counting the total number of pairs.

The two variants of the χ parameter involve different ranges of the restricted sum over chains α and β, and beads i and j in Eq. (1). χ_f measures β-strand order on an individual protofilament and alignment of the protofilament with the fibril axis, by evaluating i and j over the range from (17–21; 31–35), and over four monomer chains on each end (two independent contributions from each end involving a total of eight chains). P_f measures the nativeness of an individual protofilament, by evaluating i and j over the range from (17–35), including both β-strand regions as well as the turn connecting these regions. Because P_f is isolated to a single protofilament, each protofibril end has two values of P_f that are binned independently (four independent contributions involving eight chains total).

Free energy profiles

Based on the ensemble composed of the final structures of each of the 50 independent trajectories for each sequence and for each oligomer size, n, we can calculate equilibrium populations of structurally stable and unstable protofibrils based on population differences measured by either P_f or χ_f. For chain lengths and mutant combinations for which the population of either stable or unstable protofibrils is very small, we run an additional 100 trajectories for a total of 150 trajectories to reduce the error of our population estimates. The fraction of trajectories corresponding to $P_f > 0.7$ or $\chi_f > 0.7$ measures a population, C_n, of n-ordered monomers in a protofibril with intact end monomers and a well-defined fibril axis. This population is in equilibrium with the remaining fraction of trajectories corresponding to a protofibril with loss of structural order corresponding to $P_f < 0.7$ or $\chi_f < 0.7$, and thus measures the population C_{n-1}. We have chosen P_f and χ_f dividing surfaces of 0.7 based on the best single value of the parameters that divides the high and low chain number populations. We confirmed the choice of value by visual examination of structures with a range of P_f and χ_f values and found the values to divide ordered and disordered structures accurately.

Based on thermodynamic arguments advanced by Ferrone (28) for nucleation–polymerization reactions relevant for aggregation kinetics, at equilibrium we can estimate the change in free energy, ΔG, per unit monomer as

$$\frac{d\Delta G}{dn} = -kT\ln\left(\frac{[C_{n-1}]}{[C_n]}\right), \quad (2)$$

where n is half the number of monomers, and kT, is the Boltzmann constant multiplied by the temperature. Integration over all oligomer sizes allows us to generate a free energy curve based on C_n and C_{n-1} populations measured in our model for the different sequences.

RESULTS

We investigate the structural stability of fibril seed models for the Arctic, Dutch, and Flemish mutants ranging from 2 to 10 dimer cross sections (i.e., 4–20 monomer chains) under the C_{2z} symmetry form of the agitated fibril morphology. Each of these protofibril sizes are simulated using Langevin dynamics at a constant temperature of $T^* = 0.45$ ($T \approx$ 337K), and we monitor the amount of fibril order as a function of time. As a measure of fibril order, we define two different structural similarity parameters (see Methods). The first order parameter, P_f, measures the structural similarity of the ends of the protofilament subunits with respect to perfect fibril order. The second order parameter, χ_f, measures β-strand order over the ends of the whole protofibril, and thus is sensitive to disorder at both the level of the protofilament and the quaternary structure of the protofibril.

Fig. 2 shows the histograms of populations of P_f order for the final structures for 4, 8, and 20 peptide assemblies of the three FAD mutants with respect to the WT Aβ sequence. We see that fibril structural similarity at the level of a protofilament increases in order of FAD mutants: Flemish < Arctic < WT < Dutch at any size protofilament, regardless of the number of peptides. Because a higher concentration of peptides in solution should drive the equilibrium toward larger assemblies, the larger sized protofilaments would be more likely to be found in solutions at higher concentrations. The greater disorder by this metric for the Flemish and Arctic mutant is clearly a consequence of the glycine mutation that permits greater flexibility of the backbone dihedral angles in the N-terminal β-sheet region. The population distributions are largely no different for 8 chains versus 20 chains for the Arctic sequence, whereas there is a systematic gain of some structure for the Flemish mutant as concentration increases, although both are less fibril-like than WT. Fig. 3 shows that

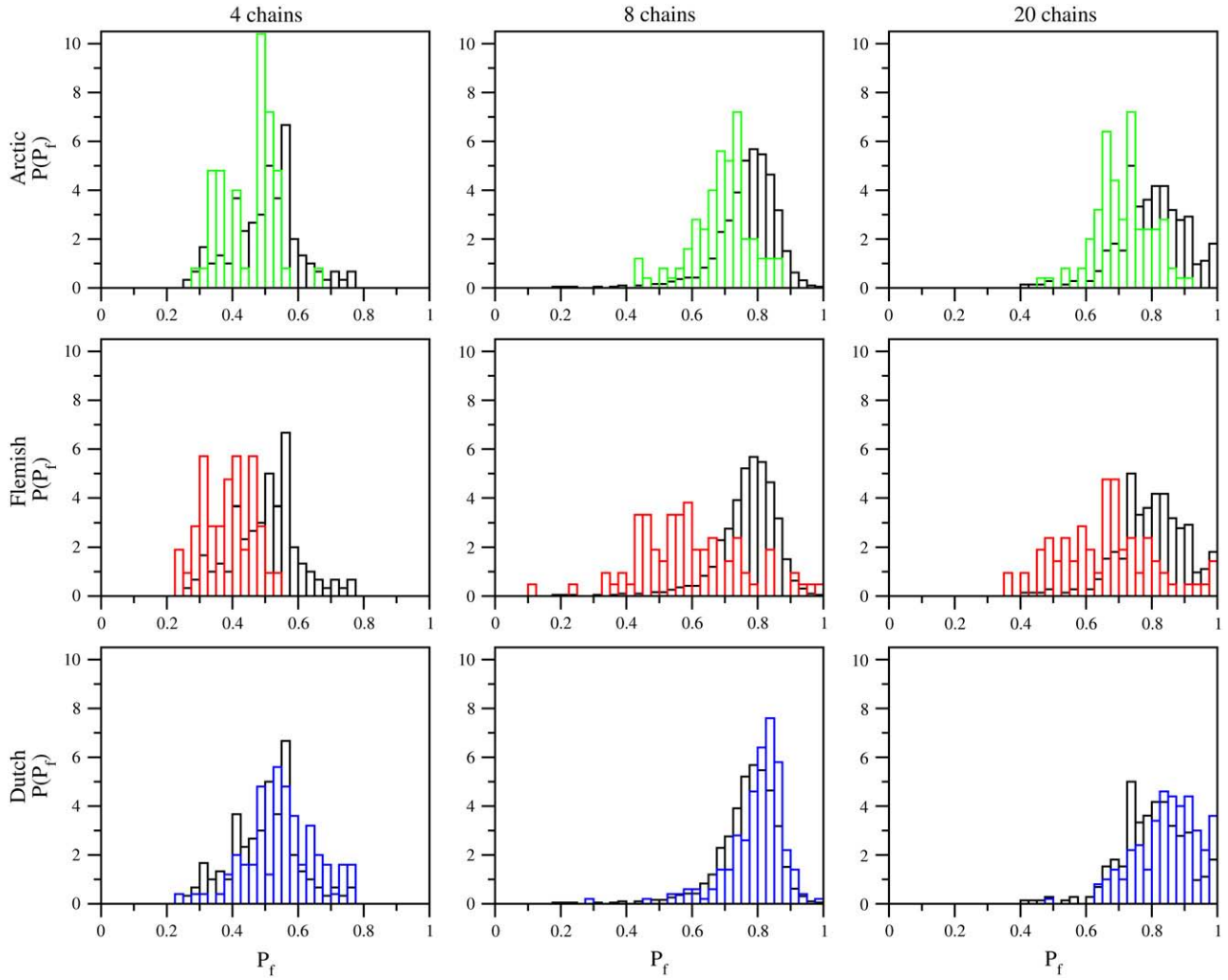

FIGURE 2 Population histograms with respect to protofilament order (P_f) for 4, 8, and 20 chains. The histograms emphasize that protofilament order increases for the FAD mutants as Flemish (*red*) < Arctic (*green*) < WT (*black*) < Dutch (*blue*), at any oligomer size.

although the Arctic mutant exhibits disorder in the turn regions, it still retains its β-strand pairings, unlike the Flemish mutant that loses the attachment of the edge monomer to the protofibril. By contrast, the Dutch sequence shows structural enhancements over WT by a primary sequence mutation that eliminates charge repulsion between peptides on the same protofilament, so that its populations are more ordered than WT at any chain assembly size. The enhancement of protofilament order for Dutch exaggerates the twist down the protofilament axis with respect to WT, as shown in Fig. 4.

The protofilament order trends for the mutant and WT sequence do not predict the trends in our χ_f metric that measures retention of order across the protofibril ends. In Fig. 5 we show the histograms of populations of χ_f for 4, 8, and 20 peptide assemblies of the three FAD mutants with respect to the WT Aβ sequence. The four-chain assemblies are equivalent

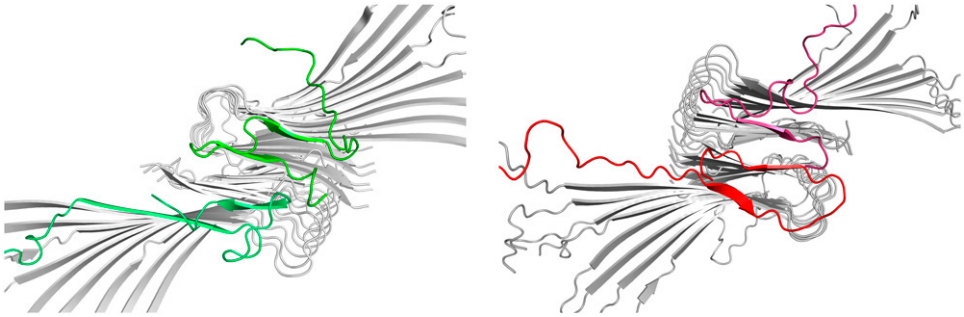

FIGURE 3 Representative protofibril structure of the Arctic and Flemish mutants. Although both FAD mutants show disorder in the turn region, the Arctic mutant (*green*) retains much better β-strand structure over the whole cross section at the end of the 5000τ-trajectories, whereas the Flemish mutant (*red*) has almost lost a monomer after the same amount of time.

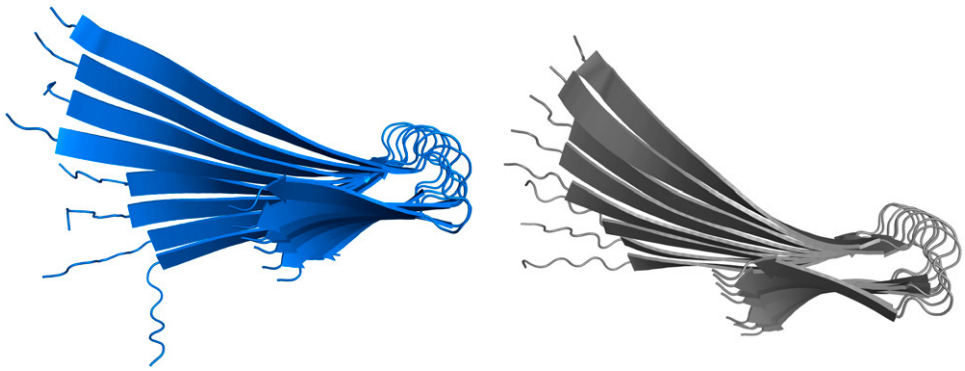

FIGURE 4 Representative protofilament structure of the Dutch mutant compared with the WT sequence. Already after only initial equilibration from the model build, the Dutch mutant (*blue*) shows a greater twist of the intermolecular β-sheet down the protofilaments with respect to WT (*black*).

among the sequences: no protofibrils are present at such low concentrations. However, fibril structural similarity at the level of a protofibril is different among the sequences at eight chains to yield a different order for FAD mutants: Flemish $<$ Dutch $<$ WT $<$ Arctic. Note that in Fig. 5, top right, the χ_f at 20 chains for Flemish mutant at 20 chains has a far lower population at $\chi_f > 0.7$, never adopting the level of protofibril order that is reached by the Arctic, Dutch, and WT mutants at eight chains.

The position of the glycine mutant results in qualitatively different behavior in the structural integrity of the protofibril. The glycine mutation at position 21 is far enough into the N-terminal β-strand to diminish fibril integrity across the whole end cross section of β-strands. By contrast, the glycine mutation at position 22 pushes the disorder nearer to the turn region, thereby retaining β-strand order over the whole cross section. In both cases, new but nonspecific stabilizing interactions between the turn region and the β-strands prevent the protofilaments from rotating with respect to each other so that both retain a well-defined protofibril axis (Fig. 3).

Although the protofilament assemblies are better formed for the Dutch mutant, the agitated fibril morphology is not a viable reference state for ordered protofibril structure (Fig. 5, *aqua*). In fact, a new polymorph (comprising 50% of the population of the 16-, 18-, and 20-chain protofibril, and ~40% for 14-chain, 35% for 12-chain, and 20% for 10-chain) is seen in which the protofilaments show a shift in register of β-strand alignment at the interface (Fig. 6). Even when this new polymorph serves as an additional reference state for fibril order (Fig. 5, *blue*), there is still some disorder for the Dutch mutant when it is compared with WT at the same number of chains, as seen by the shallower negative slope for Dutch, which is due to more rotational freedom of one protofilament with respect to another.

DISCUSSION

The kinetics of prefibrillar Arctic and WT Aβ peptides have been quantified by chromatographic methods that measure rates of appearance and disappearance of monomer and/or Aβ oligomer assemblies based on their mass (9), with no information as to their structural characteristics. A more structurally informative kinetic assay is based on Congo Red or Thioflavin T dye-binding fluorescence (49) that measures the disappearance of monomer into growing fibril assemblies that have cross β-strand order, whose long-time saturation indicates the formation of mature fibrils. However, even this kinetic measurement is not particularly sensitive to the structural details of the oligomeric assemblies that are accumulating in the measured kinetic profiles.

Our examination has shown that substantial differences in structural ensembles exist between the four different Aβ sequences based on P_f and χ_f. Both the P_f and χ_f metrics are consistent in the formation of good cross β-strand order, so that kinetic assays based on Congo Red or Thioflavin T dye-binding fluorescence are equally relevant to both of these reaction coordinates. The only difference between P_f and χ_f is that the latter assumes a higher level of structural organization so that pairs of protofilaments are well-defined with respect to the fibril axis to adopt the agitated fibril morphology. How do these structural ensembles for the different mutants connect to the observed differences in their kinetic rates of fibrillization? We make this connection under the assumption of a dynamic equilibrium between monomer and protofibril states, with the equilibrium constant allowing us to define a free energy profile as a function of protofibril assembly size (see Methods).

Fig. 7 *a* plots the free energies as a function of oligomer size for the WT and familial mutant sequences based on protofibril order, with $\chi_f > 0.7$. We find that the size of the critical nucleus shifts dramatically to a smaller number of monomer cross sections for the Arctic mutant corresponding to 6–8 chains, and exhibits a greater drive to form protofibrils with respect to WT given the smaller free energy barrier. For the Flemish mutant we find that the critical nucleus is shifted to beyond 20 chains analyzed in this study, thereby always favoring the monomer. The free energy profile for the Dutch mutant using the agitated fibril morphology relevant for WT is a poor measure of order into higher order protofilament assemblies. Even when we add the additional polymorph as a reference structure, we find that the Dutch mutant has the same critical nucleus size and slightly larger barrier to protofibril order with respect to WT. Given that the fibrillization kinetics are faster for Dutch relative to WT, this result

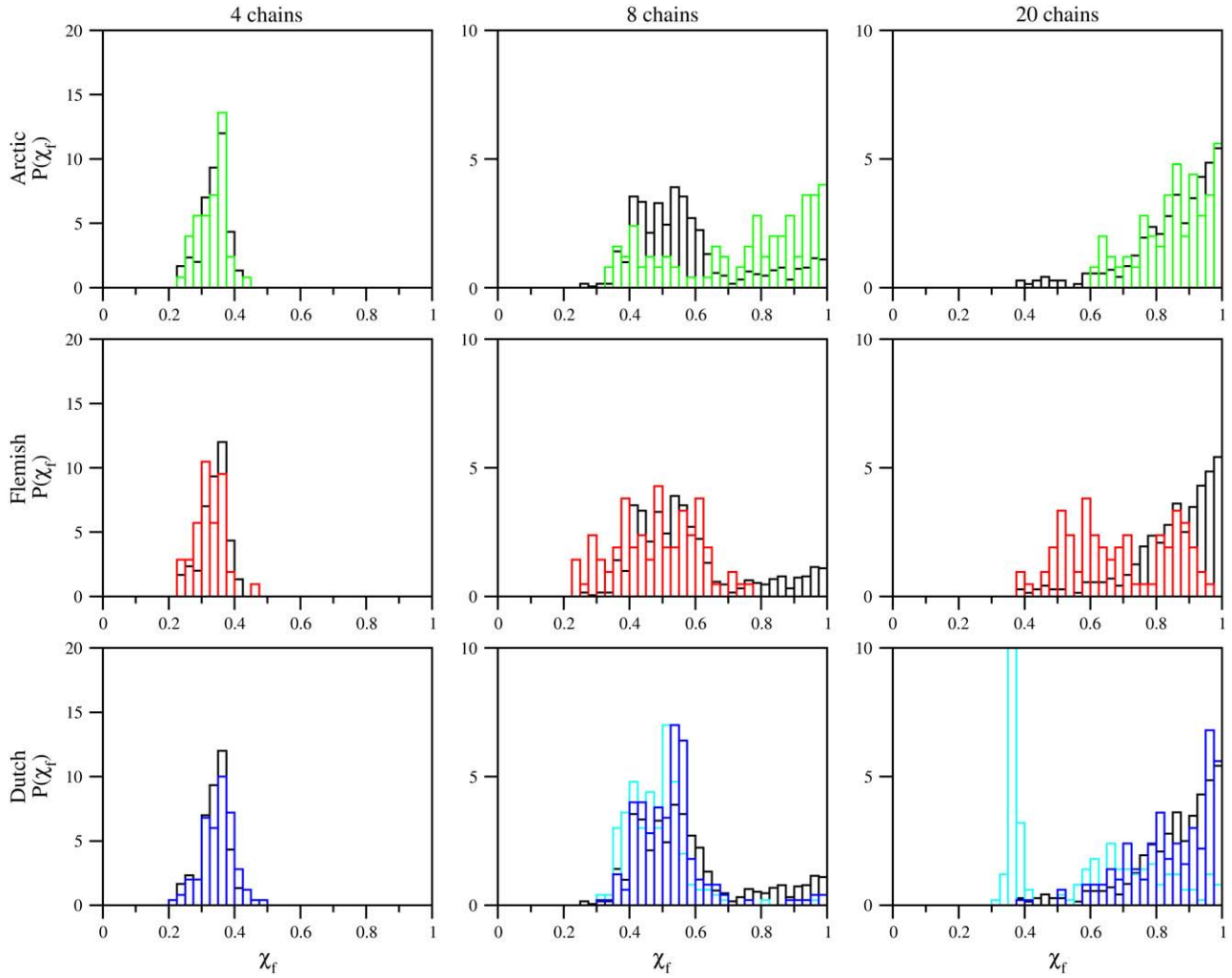

FIGURE 5 Population histograms with respect to protofibril order (χ_f) for 4, 8, and 20 chains. Although no protofibrils are present for the four-chain assemblies for any sequences, the level of protofibril structure is different among the sequences at eight chains to yield the following trend for FAD mutants: Flemish (*red*) < Dutch (*aqua*) < WT (*black*) < Arctic (*green*). Even with the addition of the Dutch polymorph as a reference state (*blue*), there is slightly more disorder for the Dutch with respect to WT.

suggests that the Dutch mutant does not favor the higher order assemblies of protofilament–protofilament organization that arise from variations of the agitated protofibril morphology.

As a measure of lower order assemblies, Fig. 7 *b* exhibits the free energies as a function of oligomer size for the WT and familial mutant sequences based on protofilament order, with $P_f > 0.7$. We see that the Dutch mutant shows the

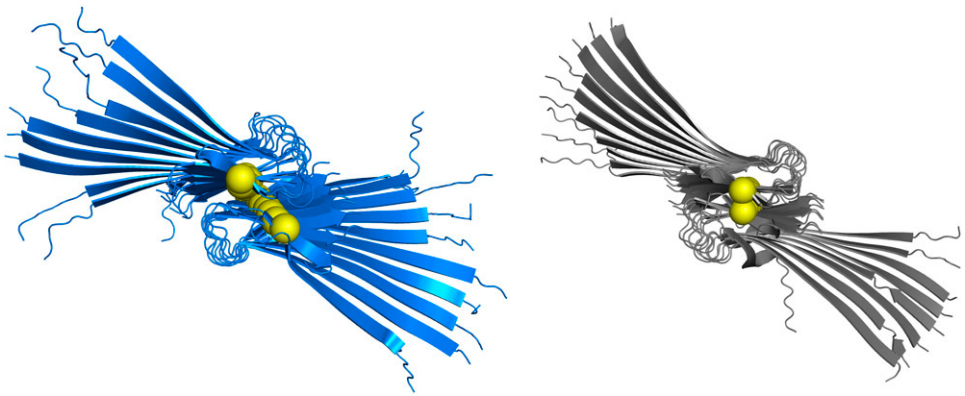

FIGURE 6 Representative protofibril structure of the Dutch mutant with respect to WT. A comparison of the Dutch polymorph (*blue*) with respect to the agitated fibril morphology (17, 31–33) favored by the WT sequence (*black*) at the end of the 5000τ-trajectories. The yellow spheres represent amino acid 33 on each monomer chain, which shows how it is displaced due to a register shift of the C-terminal β-strands at the interface under the Dutch polymorph.

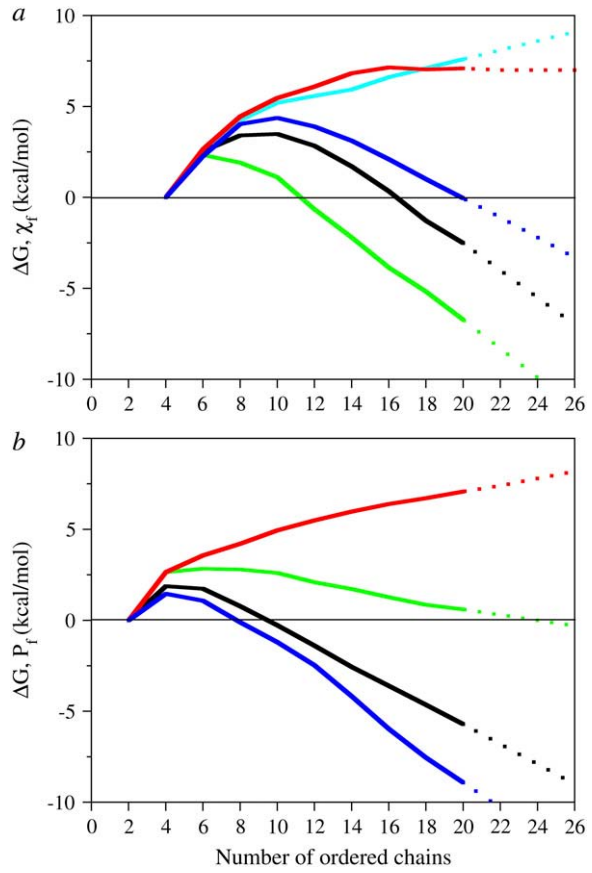

FIGURE 7 (*a*) Free energy profile for free monomer and protofibril (χ_f) equilibrium for the WT and FAD mutants. The free energy shows a maximum corresponding to the critical nucleus size of 6 chains for Arctic (*green*), 10 chains for WT (*black*), and no preferred order for either Dutch (*aqua*) or Flemish (*red*) mutants. The constant, negative slope beyond the critical nucleus is indicative of reaching a stable fibril regime in which the equilibrium shifts decidedly away from the monomer form. When the alternative polymorph for the Dutch mutant (Fig. 6) is added as a reference for fibril order (*blue*), there is now a critical nucleus of 10 chains for the E22Q mutant but with a larger free energy barrier and shallow slope indicating a slower approach to protofibril order for the Dutch mutant. (*b*) Free energy profile for free monomer and protofilament (P_f) equilibrium for the WT and FAD mutants. The free energy shows a maximum corresponding to the critical nucleus size of 6 chains for Dutch (*blue*), 6–8 chains for WT (*black*), and no preferred order for either Arctic (*green*) or Flemish (*red*) mutants. The constant, negative slope beyond the critical nucleus is indicative of reaching a stable regime in which the equilibrium favors the protofilament form, which is more strongly evident for Dutch over WT.

smallest critical nucleus and free energy barrier relative to all other sequences. The Dutch mutant preference for lower order assemblies involving only protofilaments that are not subject to the free energy barrier for ordering and aligning a two-filament cross-section fibril (48) may explain its significantly enhanced fibrillization kinetics using dye-binding assays of cross β-sheet structure. Alternatively, a higher order assembly of a substantially different polymorph other than the agitated fibril morphology may be relevant for its fibrillization mechanism. By this measure the Arctic mutant shows a flat free energy curve indicating that its structural stability arises primarily from protofilament-protofilament alignments to define a fibril axis, and that the agitated fibril assembly is a good model for this mutation. Again the Flemish mutant is disordered and never exhibits a stable protofilament regime. This result is similar to that found by all atom simulations of a Flemish mutation dimer where the A21G mutation destabilized the dimeric assembly (34). In this study, we show that this destabilization is present in ordered oligomers larger than dimers and that this local disorder leads to protofibrillar instability. Given the nature of the A21G mutation that so strongly favors the monomer over ordered cross β-sheet structure, we believe no specific alternative ordered protofibril reference state exists for the Flemish mutant.

CONCLUSIONS

We have used a coarse-grained protein model to measure structural stability trends of Aβ protofibril assemblies for WT as well as for Arctic (E22G), Dutch (E22Q), and Flemish (A21G) mutant sequences. We find that although the single point mutations are localized in the same region of the Aβ peptide, their structural ensembles are quite distinct, and the mutations can disrupt organization at the level of protofilament up through protofibril order. By measuring the equilibrium populations of monomer $\Leftrightarrow$ protofilament or monomer $\Leftrightarrow$ protofibril as a function of protofibril size, we determine free energy profiles that are consistent with the attainment of cross β-sheet structure measured by dye-binding assays, while providing better structural information on which to develop new hypotheses for experimental investigation.

We find that although both the Arctic and Flemish sequences promote greater disorder of the β-turn region of the Aβ peptide, the difference in sequence position of the glycine mutation radically alters fibril order stability. The glycine mutation at position 21 in the Flemish mutant disrupts the exterior N-terminal strand regions, thereby degrading order throughout each protofilament and at the interface between protofilaments. Regardless of the detection method (P_f versus χ_f) for cross β-sheet structure, the dynamic equilibrium strongly favors the monomeric peptide for the Flemish mutant. The greater resistance of the Flemish mutant to order into fibril assemblies of any size suggests that it is capable of both greater fragmentation into smaller oligomers that can readily diffuse, whereas at the same time possibly promoting amorphous aggregation to yield large plaques by recruiting other proteins and extracellular constituents into its more unstructured Aβ aggregates. Our results suggest it would have no definitive single fibril morphology reference state.

By contrast, the glycine mutation at position 22 is enough removed from the N-terminal strands that they retain their protofilament order, although it does increase the flexibility in the turn region of the Aβ monomer. The more flexible loop can form new contacts that stabilize the fibril at the interface so that little rotation between the protofilaments is exhibited beyond six chains. It seems likely, however, that although the

critical barrier is rapidly reached at lower concentrations than WT, the new stabilizing contacts could slow the addition of monomer beyond that point, i.e., that there is a separation between rapid attainment of small oligomers that do not translate into more rapid rates of fibrillization into large assemblies. This would be consistent with chromatography methods that measure more rapid disappearance of monomer into oligomer formations for Arctic relative to WT, but find little difference in rates of forming fibrils from these oligomer states (9).

The Dutch mutant shows an increase in protofilament order, i.e., better alignment of β-strands on the N-terminal (amino acids 17–21) and C-terminal β-strand regions (amino acids 31–35) and little disorder in the turn region. However, structural rearrangements in the monomer creates a new twist angle in the protofilament that does not allow the protofilaments to align along the fibril axis consistent with the agitated fibril structure found for the WT sequence. In fact, rearrangement between the protofilaments results in a new polymorph of the Dutch protofibril that is populated substantially. The enhanced fibrillization kinetics measured by dye-binding assays of cross β-sheet structure for the Dutch mutant may stem in part from its possible preference for lower order assemblies involving only protofilaments. Alternatively, a higher order assembly of protofilaments into a different polymorph other than the agitated fibril morphology may be relevant for its fibrillization mechanism.

We thank Robert Tycko for the atomic coordinates for his models of $A\beta_{1-40}$. K.L.K. thanks the Department of Energy Computational Science Graduate Fellowship for support and for his internship at the Berkeley Lab. N.L.F. thanks the Whitaker Foundation for a graduate research fellowship. Y.O. thanks the Guidant Foundation for a summer research fellowship. Molecular graphics for this study were created in PyMOL (DeLano Scientific, San Carlos, CA). We thank Dr. Jonathan Kohn for careful reading of the manuscript.

This work was supported in part by National Institutes of Health grant RO1 GM 070919.

REFERENCES

1. Goedert, M., and M. G. Spillantini. 2006. A century of Alzheimer's disease. *Science*. 314:777–781.
2. Dobson, C. M. 2004. Principles of protein folding, misfolding and aggregation. *Semin. Cell Dev. Biol.* 15:3–16.
3. Levy, E., M. D. Carman, I. J. Fernandez-Madrid, M. D. Power, I. Lieberburg, S. G. van Duinen, G. T. Bots, W. Luyendijk, and B. Frangione. 1990. Mutation of the Alzheimer's disease amyloid gene in hereditary cerebral hemorrhage, Dutch type. *Science*. 248:1124–1126.
4. Kamino, K., H. T. Orr, H. Payami, E. M. Wijsman, M. E. Alonso, S. M. Pulst, L. Anderson, S. Odahl, E. Nemens, J. A. White, A. D. Sadovnick, M. J. Ball, J. Kaye, A. Warren, M. McInnis, S. E. Antonarakis, J. R. Korenberg, V. Sharma, W. Kukull, E. Larson, L. L. Heston, G. M. Martin, T. D. Bird, and G. D. Schellenberg. 1992. Linkage and mutational analysis of familial Alzheimer-disease kindreds for the APP gene region. *Am. J. Hum. Genet.* 51:998–1014.
5. Hendriks, L., C. M. Vanduijn, P. Cras, M. Cruts, W. Vanhul, F. Vanharskamp, A. Warren, M. G. McInnis, S. E. Antonarakis, J. J. Martin, A. Hofman, and C. Vanbroeckhoven. 1992. Presenile-dementia and cerebral-hemorrhage linked to a mutation at codon-692 of the beta-amyloid precursor protein gene. *Nat. Genet.* 1:218–221.
6. Walsh, D. M., D. M. Hartley, M. M. Condron, D. J. Selkoe, and D. B. Teplow. 2001. In vitro studies of amyloid beta-protein fibril assembly and toxicity provide clues to the aetiology of Flemish variant (Ala(692) → Gly) Alzheimer's disease. *Biochem. J.* 355:869–877.
7. Miravalle, L., T. Tokuda, R. Chiarle, G. Giaccone, O. Bugian, F. Tagliavini, B. Frangione, and J. Ghiso. 2000. Substitutions at codon 22 of Alzheimer's abeta peptide induce diverse conformational changes and apoptotic effects in human cerebral endothelial cells. *J. Biol. Chem.* 275:27110–27116.
8. Tagliavini, F., G. Rossi, A. Padovani, M. Magoni, G. Andora, M. Sgarzi, A. Bizzi, M. Savoiardo, F. Carella, M. Morbin, G. Giaccone, and O. Bugiani. 1999. A new betaPP mutation related to hereditary cerebral hemorrhage. *Alzheimer's Reports: Vascular Factors in Alzheimer's Disease*. 2:S28.
9. Nilsberth, C., A. Westlind-Danielsson, C. B. Eckman, M. M. Condron, K. Axelman, C. Forsell, C. Stenh, J. Luthman, D. B. Teplow, S. G. Younkin, J. Naslund, and L. Lannfelt. 2001. The 'Arctic' APP mutation (E693G) causes Alzheimer's disease by enhanced A beta protofibril formation. *Nat. Neurosci.* 4:887–893.
10. Grabowski, T. J., H. S. Cho, J. P. G. Vonsattel, G. W. Rebeck, and S. M. Greenberg. 2001. Novel amyloid precursor protein mutation in an Iowa family with dementia and severe cerebral amyloid angiopathy. *Ann. Neurol.* 49:697–705.
11. Van Nostrand, W. E., J. P. Melchor, G. Romanov, K. Zeigler, and J. Davis. 2002. Pathogenic effects of cerebral amyloid angiopathy mutations in the amyloid beta-protein precursor. *In* Alzheimer's Disease: Vascular Etiology and Pathology. New York Academy of Sciences, New York. 258–265.
12. Harper, J. D., and P. T. Lansbury. 1997. Models of amyloid seeding in Alzheimer's disease and scrapie: Mechanistic truths and physiological consequences of the time-dependent solubility of amyloid proteins. *Annu. Rev. Biochem.* 66:385–407.
13. Lomakin, A., D. B. Teplow, D. A. Kirschner, and G. B. Benedek. 1997. Kinetic theory of fibrillogenesis of amyloid beta-protein. *Proc. Natl. Acad. Sci. USA*. 94:7942–7947.
14. Hortschansky, P., V. Schroeckh, T. Christopeit, G. Zandomeneghi, and M. Fandrich. 2005. The aggregation kinetics of Alzheimer's beta-amyloid peptide is controlled by stochastic nucleation. *Protein Sci.* 14:1753–1759.
15. Meinhardt, J., G. G. Tartaglia, A. Pawar, T. Christopeit, P. Hortschansky, V. Schroeckh, C. M. Dobson, M. Vendruscolo, and M. Fandrich. 2007. Similarities in the thermodynamics and kinetics of aggregation of disease-related A beta(1–40) peptides. *Protein Sci.* 16:1214–1222.
16. Morelli, L., R. Llovera, S. A. Gonzalez, J. L. Affranchino, F. Prelli, B. Frangione, J. Ghiso, and E. M. Castano. 2003. Differential degradation of amyloid beta genetic variants associated with hereditary dementia or stroke by insulin-degrading enzyme. *J. Biol. Chem.* 278:23221–23226.
17. Petkova, A. T., R. D. Leapman, Z. H. Guo, W. M. Yau, M. P. Mattson, and R. Tycko. 2005. Self-propagating, molecular-level polymorphism in Alzheimer's beta-amyloid fibrils. *Science*. 307:262–265.
18. Stern, E. A., B. J. Bacskai, G. A. Hickey, F. J. Attenello, J. A. Lombardo, and B. T. Hyman. 2004. Cortical synaptic integration in vivo is disrupted by amyloid-beta plaques. *J. Neurosci.* 24:4535–4540.
19. Bucciantini, M., E. Giannoni, F. Chiti, F. Baroni, L. Formigli, J. S. Zurdo, N. Taddei, G. Ramponi, C. M. Dobson, and M. Stefani. 2002. Inherent toxicity of aggregates implies a common mechanism for protein misfolding diseases. *Nature*. 416:507–511.
20. Stefani, M., and C. M. Dobson. 2003. Protein aggregation and aggregate toxicity: new insights into protein folding, misfolding diseases and biological evolution. *J. Mol. Med.* 81:678–699.
21. Braak, H. and E. Braak. 1998. Evolution of neuronal changes in the course of Alzheimer's disease. *J. Neural. Transm. Suppl.* 53:127–40.
22. Lambert, M. P., A. K. Barlow, B. A. Chromy, C. Edwards, R. Freed, M. Liosatos, T. E. Morgan, I. Rozovsky, B. Trommer, K. L. Viola, P. Wals, C. Zhang, C. E. Finch, G. A. Krafft, and W. L. Klein. 1998. Diffusible,

nonfibrillar ligands derived from A beta(1–42) are potent central nervous system neurotoxins. *Proc. Natl. Acad. Sci. USA.* 95:6448–6453.

23. Stine, W. B., K. N. Dahlgren, G. A. Krafft, and M. J. LaDu. 2003. In vitro characterization of conditions for amyloid-beta peptide oligomerization and fibrillogenesis. *J. Biol. Chem.* 278:11612–11622.
24. Klyubin, I., D. M. Walsh, W. K. Cullen, J. V. Fadeeva, R. Anwyl, D. J. Selkoe, and M. J. Rowan. 2004. Soluble Arctic amyloid beta protein inhibits hippocampal long-term potentiation in vivo. *Eur. J. Neurosci.* 19:2839–2846.
25. Dolphin, G. T., P. Dumy, and J. Garcia. 2006. Control of amyloid beta-peptide protofibril formation by a designed template assembly. *Angew. Chem. Int. Ed.* 45:2699–2702.
26. Lomakin, A., D. S. Chung, G. B. Benedek, D. A. Kirschner, and D. B. Teplow. 1996. On the nucleation and growth of amyloid beta-protein fibrils: Detection of nuclei and quantitation of rate constants. *Proc. Natl. Acad. Sci. USA.* 93:1125–1129.
27. Sciarretta, K. L., D. J. Gordon, A. T. Petkova, R. Tycko, and S. C. Meredith. 2005. A beta 40-Lactam(D23/K28) models a conformation highly favorable for nucleation of amyloid. *Biochemistry.* 44:6003–6014.
28. Ferrone, F. 1999. Analysis of protein aggregation kinetics. *In* Amyloid, Prions, and Other Protein Aggregates. Academic Press, San Diego. 256–274.
29. Nguyen, P. H., M. S. Li, G. Stock, J. E. Straub, and D. Thirumalai. 2007. Monomer adds to preformed structured oligomers of A beta-peptides by a two-stage dock-lock mechanism. *Proc. Natl. Acad. Sci. USA.* 104:111–116.
30. Tarus, B., J. E. Straub, and D. Thirumalai. 2005. Probing the initial stage of aggregation of the A beta(10–35)-protein: Assessing the propensity for peptide dimerization. *J. Mol. Biol.* 345:1141–1156.
31. Baumketner, A., and J. E. Shea. 2006. Folding landscapes of the Alzheimer amyloid-beta(12–28) peptide. *J. Mol. Biol.* 362:567–579.
32. Buchete, N. V., and G. Hummer. 2007. Structure and dynamics of parallel β-sheets, hydrophobic core, and loops in Alzheimer's Aβ-fibrils. *Biophys. J.* 92:3032–3039.
33. Hills, R. D., and C. L. Brooks. 2007. Hydrophobic cooperativity as a mechanism for amyloid nucleation. *J. Mol. Biol.* 368:894–901.
34. Huet, A., and P. Derreumaux. 2006. Impact of the mutation A21G (Flemish variant) on Alzheimer's β-amyloid dimers by molecular dynamics simulations. *Biophys. J.* 91:3829–3840.
35. Ma, B. Y., and R. Nussinov. 2002. Stabilities and conformations of Alzheimer's beta-amyloid peptide oligomers (A beta(16–22′) A beta(16–35′) and A beta(10–35)): Sequence effects. *Proc. Natl. Acad. Sci. USA.* 99:14126–14131.
36. Tarus, B., J. E. Straub, and D. Thirumalai. 2006. Dynamics of Asp23-Lys28 salt-bridge formation in A beta(10–35) monomers. *J. Am. Chem. Soc.* 128:16159–16168.
37. Urbanc, B., L. Cruz, F. Ding, D. Sammond, S. Khare, S. V. Buldyrev, H. E. Stanley, and N. V. Dokholyan. 2004. Molecular dynamics simulation of amyloid β-dimer formation. *Biophys. J.* 87:2310–2321.
38. Xu, Y. C., J. J. Shen, X. M. Luo, W. L. Zhu, K. X. Chen, J. P. Ma, and H. L. Jiang. 2005. Conformational transition of amyloid beta-peptide. *Proc. Natl. Acad. Sci. USA.* 102:5403–5407.
39. Favrin, G., A. Irback, and S. Mohanty. 2004. Oligomerization of amyloid A β(16–22) peptides using hydrogen bonds and hydrophobicity forces. *Biophys. J.* 87:3657–3664.
40. Klimov, D. K., J. E. Straub, and D. Thirumalai. 2004. Aqueous urea solution destabilizes A beta(16–22) oligomers. *Proc. Natl. Acad. Sci. USA.* 101:14760–14765.
41. Klimov, D. K., and D. Thirumalai. 2003. Dissecting the assembly of A beta(16–22) amyloid peptides into antiparallel beta sheets. *Structure.* 11:295–307.
42. Wei, G. H., and J. E. Shea. 2006. Effects of solvent on the structure of the Alzheimer amyloid-β(25–35) peptide. *Biophys. J.* 91:1638–1647.
43. Zheng, J., H. Jang, B. Ma, C. J. Tsai, and R. Nussinov. 2007. Modeling the Alzheimer A$\{\beta\}$17–42 fibril architecture: tight intermolecular sheet-sheet association and intramolecular hydrated cavities. *Biophys. J.* 93:3046–3057.
44. Balbach, J. J., A. T. Petkova, N. A. Oyler, O. N. Antzutkin, D. J. Gordon, S. C. Meredith, and R. Tycko. 2002. Supramolecular structure in full-length Alzheimer's β-amyloid fibrils: evidence for a parallel β-sheet organization from solid-state nuclear magnetic resonance. *Biophys. J.* 83:1205–1216.
45. Petkova, A. T., Y. Ishii, J. J. Balbach, O. N. Antzutkin, R. D. Leapman, F. Delaglio, and R. Tycko. 2002. A structural model for Alzheimer's beta-amyloid fibrils based on experimental constraints from solid state NMR. *Proc. Natl. Acad. Sci. USA.* 99:16742–16747.
46. Petkova, A. T., W. M. Yau, and R. Tycko. 2006. Experimental constraints on quaternary structure in Alzheimer's beta-amyloid fibrils. *Biochemistry.* 45:498–512.
47. Yap, E. H., N. L. Fawzi, and T. Head-Gordon. 2008. A coarse-grained alpha-carbon protein model with anisotropic hydrogen-bonding. *Proteins.* 70:626–638.
48. Fawzi, N. L., Y. Okabe, E. H. Yap, and T. Head-Gordon. 2007. Determining the critical nucleus and mechanism of fibril elongation of the Alzheimer's A beta(1–40) peptide. *J. Mol. Biol.* 365:535–550.
49. Westermark, G. T., K. H. Johnson, and P. Westermark. 1999. Staining methods for identification of amyloid in tissue. *In* Amyloid, Prions, and Other Protein Aggregates. Academic Press, San Diego. 3–25.
50. Brown, S., N. J. Fawzi, and T. Head-Gordon. 2003. Coarse-grained sequences for protein folding and design. *Proc. Natl. Acad. Sci. USA.* 100:10712–10717.
51. Brown, S., and T. Head-Gordon. 2004. Intermediates and the folding of proteins L and G. *Protein Sci.* 13:958–970.
52. Fawzi, N. L., V. Chubukov, L. A. Clark, S. Brown, and T. Head-Gordon. 2005. Influence of denatured and intermediate states of folding on protein aggregation. *Protein Sci.* 14:993–1003.
53. Sorenson, J. M., and T. Head-Gordon. 1999. Redesigning the hydrophobic core of a model beta-sheet protein: destabilizing traps through a threading approach. *Proteins Struct. Funct. Genet.* 37:582–591.
54. Sorenson, J. M., and T. Head-Gordon. 2000. Matching simulation and experiment: a new simplified model for simulating protein folding. *J. Comput. Biol.* 7:469–481.
55. Sorenson, J. M., and T. Head-Gordon. 2002. Protein engineering study of protein L by simulation. *J. Comput. Biol.* 9:35–54.
56. Sikorski, P., and E. Atkins. 2005. New model for crystalline polyglutamine assemblies and their connection with amyloid fibrils. *Biomacromolecules.* 6:425–432.
57. Andersen, H. C. 1983. RATTLE–a velocity version of the shake algorithm for molecular-dynamics calculations. *J. Comput. Phys.* 52: 24–34.